NASA TM-87755

NASA-TM-87755 19860021223

NASA Technical Memorandum 87755

EXPERIMENTAL AND NUMERICAL RESULTS FOR A GENERIC AXISYMMETRIC SINGLE-ENGINE AFTERBODY WITH HORIZONTAL AND VERTICAL TAILS AT TRANSONIC SPEEDS

James R. Burley, II, John R. Carlson,
and William P. Henderson

August 1986

LIBRARY COPY

SEP 10 1986

LANGLEY RESEARCH CENTER
LIBRARY, NASA
HAMPTON, VIRGINIA

National Aeronautics and
Space Administration

Langley Research Center
Hampton, Virginia 23665

3 1176 01316 0131

SUMMARY

An experimental investigation has been conducted in the Langley 16-Foot Transonic Tunnel to measure static pressures on the afterbody, nozzle, and tails of an axisymmetric single-engine configuration representative of today's fighter aircraft. Data were recorded at Mach numbers 0.6, 0.9, and 1.2. Nozzle pressure ratio was varied from 1.0 to 8.0 and angle-of-attack was varied from -3 deg. to 9 deg. at each Mach number. Three empennage arrangements were tested (aft, forward, staggered) with a single dry power nozzle. Detailed pressure data were obtained for these configurations for which force and moment data had been previously recorded. Two numerical codes were used to predict the static pressure coefficients on the staggered empennage arrangement. Comparisons were made between the experimental pressure coefficients and numerical results from both codes.

INTRODUCTION

Because of the large effect of tail surfaces on afterbody/nozzle drag, an extensive experimental program to determine these effects on single-engine fighter configurations is being conducted at the Langley Research Center. Detailed experimental data can be found in references 1, 2, and 3 for a generic single-engine configuration representative of today's fighter aircraft. These data show how area ruling, tail arrangement and tail span can effect forces and moments acting on the afterbody and nozzle. Tail interference effects can account for nearly 40% of the total drag at transonic speeds depending on the empennage arrangement (ref. 2). However, a lack of detailed flow data on and around the afterbody, nozzle, and tails has made it very difficult to determine the origin of this interference and explain why it occurs. The detailed static pressure data needed to analyze the flow characteristics over the nozzle/afterbody would also be useful in validating theoretical codes designed to predict this complex flowfield. A recent AGARD assessment of prediction capabilities for afterbody flows (ref. 4) indicated that a good prediction of boattail pressure drag was not a good criteria for code validation. Instead, static pressure distributions should be used to verify code predictions. Reference 4 also pointed out the lack of experimental static pressure data available for this use. This paper describes an experimental investigation aimed at filling the need for static pressure data on complex afterbody configurations with and without tails. In addition, two theoretical codes (one production, one developmental) were used to predict static pressure coefficients on the afterbody and nozzle.

SYMBOLS

b	span(root to tip) of baseline tail surface (used for both vertical and horizontal tails), in
C_p	static-pressure coefficient, $(p-p_\infty)/q_\infty$
L	model length, 71.70 in

N86-30695 #

M	Mach number
NPR	nozzle pressure ratio
p	local static pressure, psi
p_∞	freestream static pressure, psi
q_∞	freestream dynamic pressure, psi
R	radial coordinate, in
x	streamwise coordinate, in
y	spanwise coordinate, in
α	angle-of-attack, deg
ϕ	meridian angle, positive counter-clockwise, deg

EXPERIMENTAL APPARATUS AND TEST PROCEDURES

The investigation was conducted in the NASA Langley 16-Foot Transonic Tunnel, a single-return atmospheric tunnel with a slotted octagonal test section and continuous air exchange. A complete description of this facility can be found in reference 5. Data were recorded at Mach numbers 0.6, 0.9, and 1.2. At each Mach number, an angle-of-attack and nozzle pressure ratio(NPR) sweep were made. Angle-of-attack varied from -3 deg. to 9 deg. while NPR varied from 1.0 (jet-off) to 8.0. Reynolds number based on the model length (L) varied from approximately 6.6×10^7 at M = 0.6 to 7.9×10^7 at M = 1.2. To insure a turbulent boundary-layer, transition strips of no. 100 grit were placed on the leading edges of the tails and the nose of the model. The nozzle exhaust flow was simulated by a continuous flow of clean dry air at a controlled temperature of 70°F.

A sketch of the sting-strut-supported single-engine model is presented in figure 1. The overall model arrangement represents a typical single-engine fighter aft-end. The axisymmetric nozzle simulates a dry power subsonic cruise mode of operation while the horizontal and vertical tails are sized to represent a typical fighter empennage arrangement. Three empennage arrangements were tested; aft, forward, and staggered. Figures 2(a) and 2(b) fully describe the horizontal and vertical tails. Figures 3(a) and 3(b) give the afterbody and nozzle dimensions as well as pressure orifice locations. Photographs of the model installed in the wind tunnel are presented in figure 4. The tails are shown in the staggered empennage arrangement.

INSTRUMENTATION

Forces and moments were not measured during this test since references 1, 2, and 3 fully document them for the configurations of this test. The stagnation pressure and temperature of the jet exhaust were measured just ahead of the nozzle

throat as shown in fig. 1. Over 300 static pressure orifices were located on the model.

THEORETICAL METHODS

Two prediction methods for afterbody flow problems were examined. The first method was a well known production code called VSAERO while the second method was a viscous-inviscid interaction scheme developed by Wilmoth and Putnam (ref. 6).

VSAERO (Vortex Separation Aerodynamic Program) is a surface singularity program which utilizes quadrilateral panels to represent arbitrary three-dimensional bodies. Source and doublet singularities are distributed in a piecewise constant fashion on each panel. Neumann boundary conditions are applied to determine the source strengths while Dirichlet boundary conditions are applied to determine the doublet strengths. The jet wake is modeled using doublet sheets with a linear variation in doublet strength in the streamwise direction. Viscous effects are accounted for by performing a two-dimensional integral boundary-layer calculation along surface streamlines determined from an initial potential flow calculation. The boundary-layer thickness is simulated by surface transpiration from which a new potential flow solution is derived. VSAERO is used primarily for predicting subsonic aerodynamic characteristics and is a well known and highly used code.

The viscous-inviscid interaction scheme developed by Wilmoth and Putnam is illustrated in figure 5. RAXJET (ref. 7) is a viscous-inviscid method for isolated axisymmetric boattails and is used to calculate an effective body geometry accounting for boundary-layer displacement and jet plume effects. Figure 6 illustrates the flowfield which RAXJET attempts to solve by patching together several numerical methods each designed to calculate a particular part of the flow. This type of jet flowfield modeling has proven to be very accurate for isolated boattail geometries. For the tails, an integral boundary-layer calculation is performed in strip fashion. The resulting effective body and tails is input to the inviscid full-potential finite volume transonic code FL030V. This developmental code utilizes the method of Caughey and Jameson (ref. 8) which is based upon the simple form of the quasilinear potential equation and a mesh generation technique which wraps a C-type grid around the body and tails. Ideally the boundary-layer calculation of this method would be repeated to convergence as shown by the dashed line in figure 5, however, for the calculations shown in this paper only one pass through this procedure was performed. The bounday-layer iteration scheme requires a method for calculating the boundary-layer on a three-dimensional surface. RAXJET assumed axisymmetric flow over the body which was an excellent initial calculation but could not be applied to the body and tails because the axisymmetric flow assumption was no longer valid. Since the boundary-layer on the body and tails were computed separately, tail interference effects were not included in these calculations.

EXPERIMENT/THEORY COMPARISONS

All comparisons between predicted and measured static pressure coefficient data were done at 0^{o} angle-of-attack for the body without tails and the staggered empennage arrangement. However, the experimental database does include data for other empennage arrangements and angles-of-attack.

Body only, tails off.- Figure 7 presents FL030V and VSAERO results at Mach number 0.9 and NPR 5.0. The experimental data were taken from the $\phi = 18^{0}$ row however, any row could have been used due to the symmetry of this configuration. The experimental pressure data indicate that the flow accelerates gradually over the afterbody and nozzle and then rapidly decelerates near the nozzle exit. The entire flowfield remained subsonic and the low velocities near the nozzle exit were caused by jet plume blockage effects. The pressure recovery and positive pressure coefficients on the nozzle reduced the nozzle pressure drag to essentially zero for this configuration. Both codes accurately predict the afterbody pressure coefficients, however, predictions for the nozzle region show some disagreement. The flow about the nozzle is significantly influenced by jet entrainment and viscous effects. For this reason the FL030V results which model these phenomena through RAXJET are superior to the VSAERO results. In VSAERO the jet wake is modeled using doublet sheets with a linear variation in doublet strength in the streamwise direction. The "velocity jump" that occurs across the doublet sheet is calculated by the program. Figure 6 indicates that this type of modeling is inferior to the viscous-inviscid modeling used in RAXJET. The VSAERO results are inviscid and very sensitive to slop discontinuities in the geometry, which may explain why the minimum C_p occurs at the point of maximum nozzle surface curvature. However, upon closer inspection no discontinuities could be found in the mathematical model of the nozzle. Similiar results were obtained at M = 0.6 and NPR = 3.0.

Staggered empennage arrangement.- The staggered empennage arrangement places the root leading edge of the horizontal tails at x/l = 0.78 and the trailing edge at x/l = 0.96. The vertical tail root leading edge is at x/l = 0.64 and the trailing is at x/l = 0.87. The photographs in figure 4 may help in visualizing this arrangement. The staggered tail arrangement was choosen because it produced the least tail interference at transonic conditions of the three configurations tested in reference 2. This is substantiated by the data of reference 3 which shows that the interference drag is nearly zero for the staggered tails. Other tail arrangements such as the horizontal and vertical tails aft, produced very large interference drag. Figure 8 compares the numerical results with the experimental data at M = 0.6, NPR = 3.0, and $\phi = 18^{0}$. The experimental results indicate that the flow slows down in the vicinity of the vertical tail leading edge and then accelerates towards the maximum thickness of the vertical tail. Although the presence of the tails are evident in the data, interference effects are negligible. The numerical results show good agreement with the data except in the vicinity of the nozzle. In this region strong viscous effects caused by the jet predominate. VSAERO attempts to model this flowfield with doublet sheets of varying strength. FL030V on the other hand, relies on the RAXJET calculations for an effective body which accounts for the effects of jet entrainment and flow separation. As a result, the FL030V calculations better predict the experimental data near the nozzle. Ahead of the nozzle, the VSAERO calculations more accurately predict the experimental data, however, the differences between the VSAERO and FL030V results are small.

At M = 0.9 tail interference effects become significant as shown in figure 9. Data are presented for NPR = 5.0 and $\phi = 18^{0}$. The experimental data show some regions of the flow approaching sonic conditions, however no flow separation appears to be present. The VSAERO results are inviscid since a viscous solution at M = 0.9 could not be obtained due to divergence of the calculation. At $\phi = 18^{0}$, the nearness of the vertical tail is evident in these data. The stagnation occuring at the leading edge of the vertical tail can be seen as a local pressure coefficient peak at x/l = 0.64. This peak is over predicted by VSAERO and underpredicted by

FL030V. The VSAERO results tend to overpredict the tail installation effects over the entire pressure distribution. This was expected since the calculations were inviscid. The FL030V calculations did account for viscous effects but the boundary-layer on the body and tails were computed separately as two-dimensional elements so that the influence of the tails are not included in the body boundary-layer calculation. As a result, the FL030V calculations show some influence of the tails (potential) but fail to predict the severity of the interference (viscous) caused by the tails. A full three-dimensional boundary-layer calculation would significantly improve the capability of the viscous-inviscid interaction scheme by providing FL030V with an effective body geometry which accounts for the presence of the tails.

In figure 10 experimental data and numerical results are shown for $\phi = 72^{o}$ which is near the left horizontal tail. As in figure 7, the Mach number is 0.9 and the NPR is 5.0. The data are similiar to the $\phi = 18^{o}$ data because the stagnation at the leading edge of the horizontal tail produces a local pressure coefficient maxima just as the vertical tail did. However, the staggered empennage arrangement places the horizontal tail further aft (leading edge located at $x/l = .78$ and trailing edge at $x/l = .96$) in a region of higher velocity flow so that the pressure coefficient peak is not as significant. The presence of the vertical tail can still be seen in the $\phi = 72^{o}$ data as a local pressure coefficient maxima at $x/l = 0.64$. This seems to indicate that the interference is widespread covering the entire area between the horizontal and vertical tails. The numerical results are similiar to the $\phi = 18^{o}$ data with one exception. The vertical tail effects at $\phi = 72^{o}$ are not predicted. As a result, the theoretical data would indicate less interference than is actually present.

CONCLUSIONS

The experimental pressure coefficient database generated by the investigation described compliments the existing force and moment database and will contribute to the understanding of the tail interference problem as well as aid in theoretical code development and validation. The numerical results of this investigation lead to the following conclusions:

(1) The type of jet wake modeling used in VSAERO did not accurately model the entrainment effects thus reducing the usefulness of the code to afterbody/nozzle propulsion installations

(2) The viscous-inviscid computational model showed promise, but requires a fully three-dimensional boundary-layer calculation to accurately predict tail interference effects.

REFERENCES

1. Berrier, Bobby L.: Effect of Nonlifting Empennage Surfaces on Single-Engine Aftbody/Nozzle Drag at Mach Numbers from 0.50 to 2.2. NASA TN D-8326, 1977.

2. Burley, James R. II; and Berrier, Bobby L.: Investigation of Installation Effects on Single-Engine Convergent-Divergent Nozzles. NASA TP-2078, 1982.

3. Burley, James R. II; and Berrier, Bobby L.: Effects of Tail Span and Empennage Arrangement on Drag of a Typical Single-Engine Fighter Aft End. NASA TP-2352, 1984.

4. Putnam, L. E.; and Bissinger, N. C.: Results of AGARD Assessment of Prediction Capabilities for Nozzle Afterbody Flows. AIAA Paper No. 85-1464, 1985.

5. Peddrew, K. H., compiler: A User's Guide to the Langley 16-Foot Transonic Tunnel, NASA TM-83186, 1981.

6. Putnam, L. E.; and Wilmoth, Richard G.: Subsonic/Transonic Prediction Capabilities for Nozzle/Afterbody Configurations. AIAA Paper No. 84-0192, 1984.

7. Wilmoth, Richard, G.: RAXJET: A Computer Program for Predicting Transonic Axisymmetric Flow Over Nozzle Afterbodies With Supersonic Jet Exhausts. NASA TM-83235, 1982.

8. Jameson, A.; and Caughey, D.: A Finite Volume Method for Transonic Potential Flow Calculation. AIAA Paper No. 77-635, 1977.

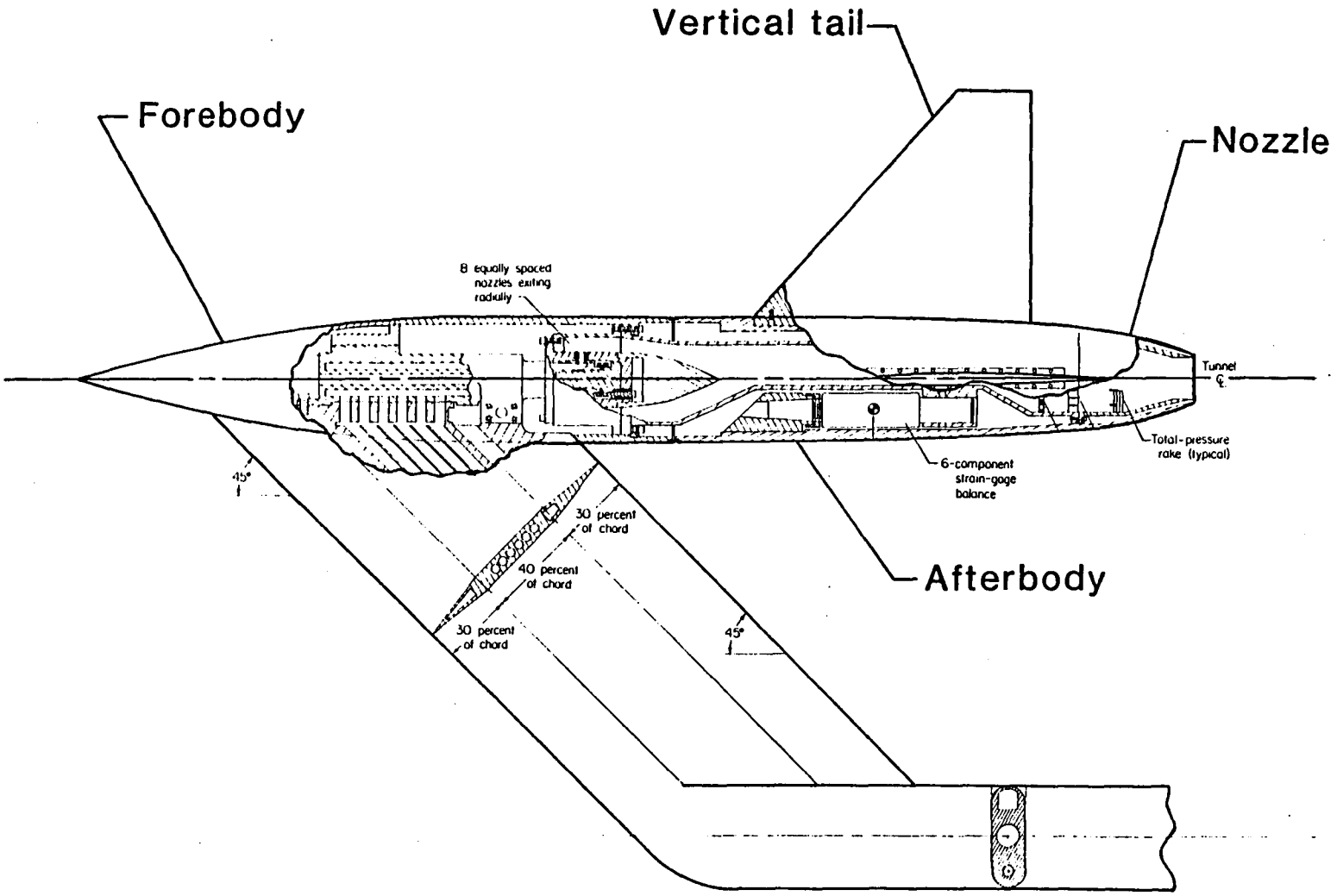

Figure 1. - Sketch of the sting-strut-supported single-engine model.

Orifice	y/b	x/c	x, in.	y, in.
1	0.1	.05	0.583	1.015
2		.10	1.165	
3		.20	2.330	
4		.30	3.495	
5		.40	4.660	
6		.50	5.825	
7		.60	6.990	
8		.70	8.15	
9		.80	9.320	
10		.90	10.485	
11	0.2	.05	0.580	2.030
12		.10	1.060	
13		.20	2.12	
14		.30	3.18	
15		.40	4.240	
16		.50	5.300	
17		.60	6.360	
18		.70	7.420	
19		.80	8.480	
20		.90	9.540	

Note: Looking upstream, station 1 is on the bottom side of the left horizontal tail and station 2 is on the top side of the right horizontal tail. The left and right horizontal tails are interchangeable.

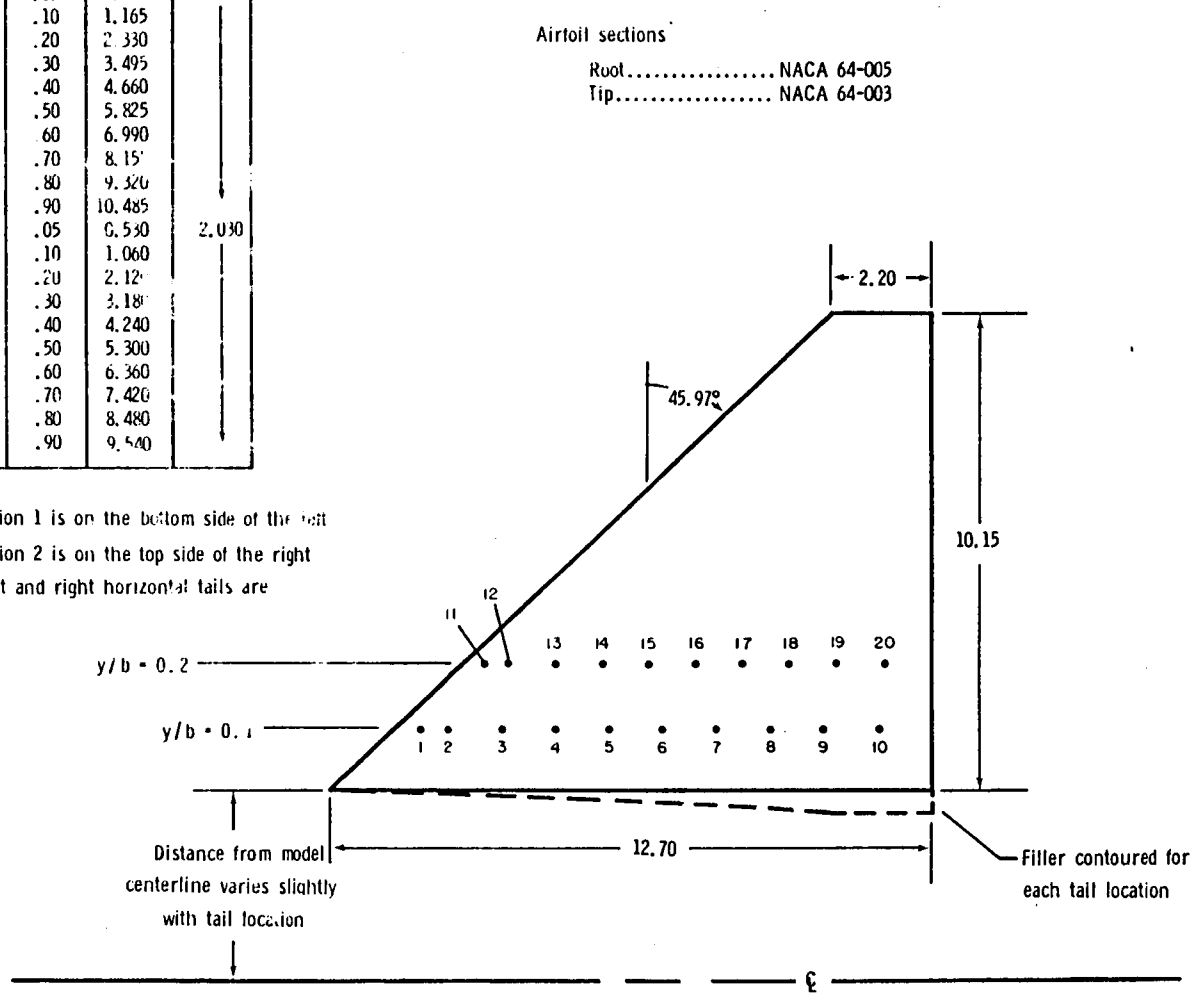

(a) Horizontal tails.

Figure 2.- Dimensions for the horizontal and vertical tails including pressure orifice locations.

Orifice	y/b	x/c	x, in	y, in.
1	0.1	.05	0.760	1.326
2		.10	1.518	
3		.20	3.040	
4		.30	4.550	
5		.40	6.070	
6		.50	7.590	
7		.60	9.110	
8		.70	10.630	
9		.80	12.140	
10		.90	13.660	
11	0.2	.05	0.700	2.6522
12		.10	1.400	
13		.20	2.790	
14		.30	4.190	
15		.40	5.580	
16		.50	6.980	
17		.60	8.380	
18		.70	9.770	
19		.80	11.170	
20		.90	12.560	

Note: Station 1 and 2 are on the left side of the vertical tail when looking upstream.

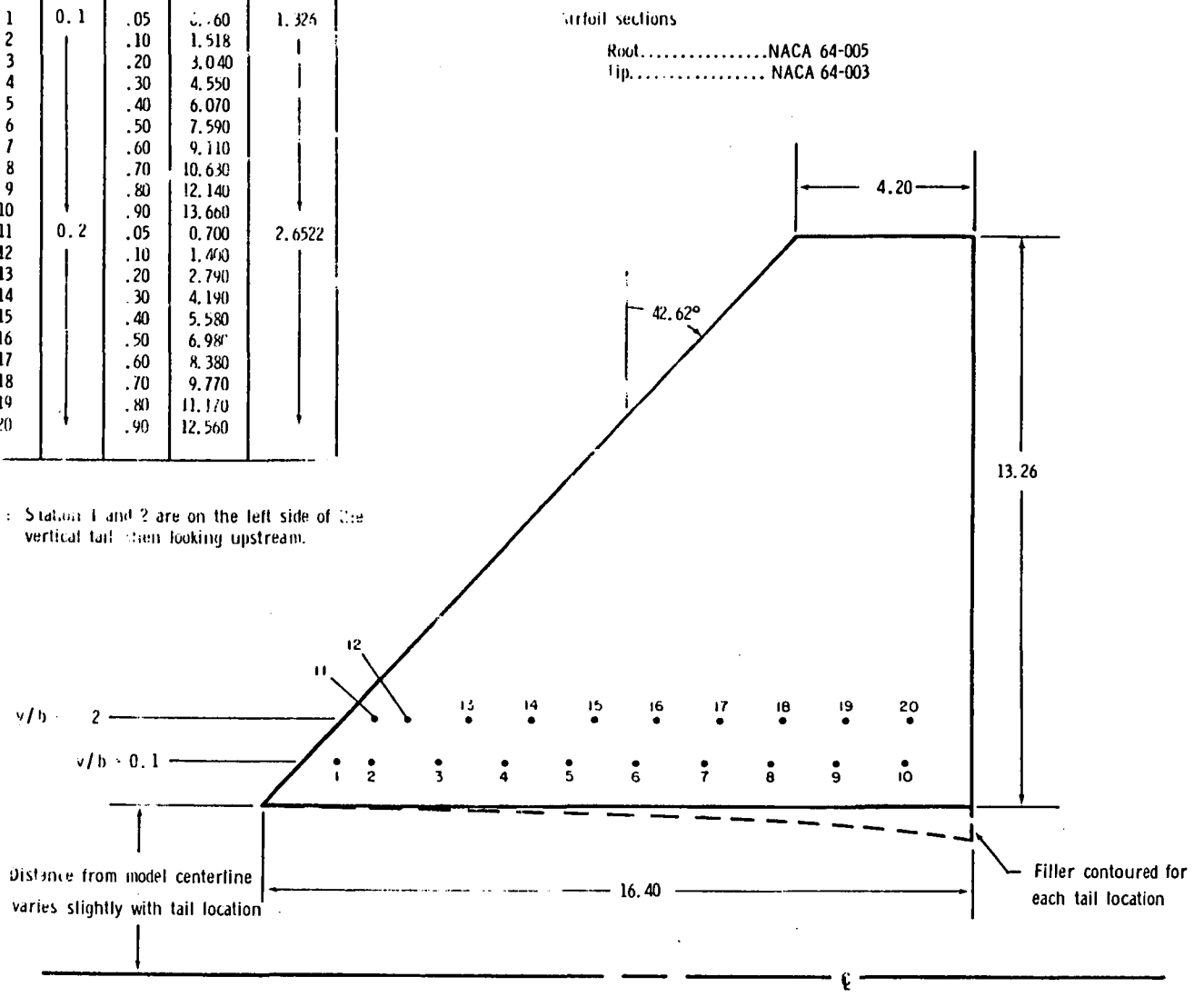

(b) Vertical tail.

Figure 2.- Concluded.

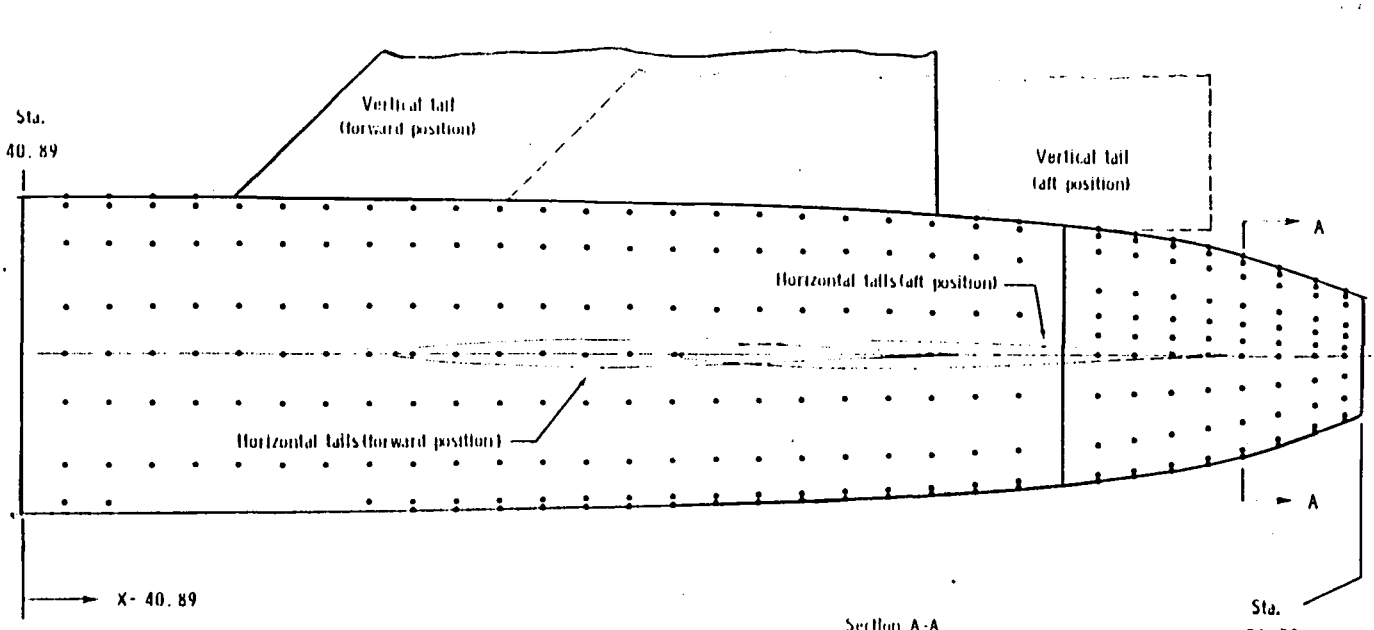

Afterbody/nozzle external geometry

X, in.	R, in.
40.888	3.670
42.888	3.664
44.888	3.654
46.888	3.636
48.888	3.612
50.888	3.580
52.888	3.539
54.888	3.488
56.888	3.425
58.888	3.348
60.888	3.248
61.388	3.217
61.888	3.184
62.388	3.147
62.888	3.108
63.488	3.056
64.888	3.000
65.700	2.919
67.181	2.726
67.700	2.635
68.700	2.400
69.700	2.098
70.700	1.750
71.700	1.374

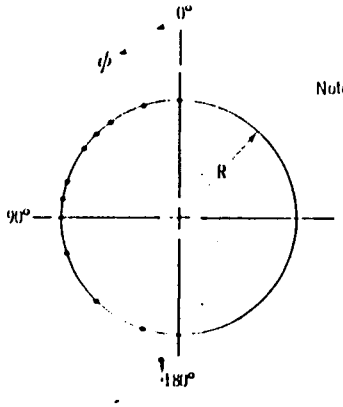

Note: pressure taps are on the left side of the afterbody and nozzle when looking upstream.

(a) Afterbody and nozzle geometry.

Figure 3.- Dimensions for the afterbody and nozzle including pressure orifice locations and coordinate system orientation.

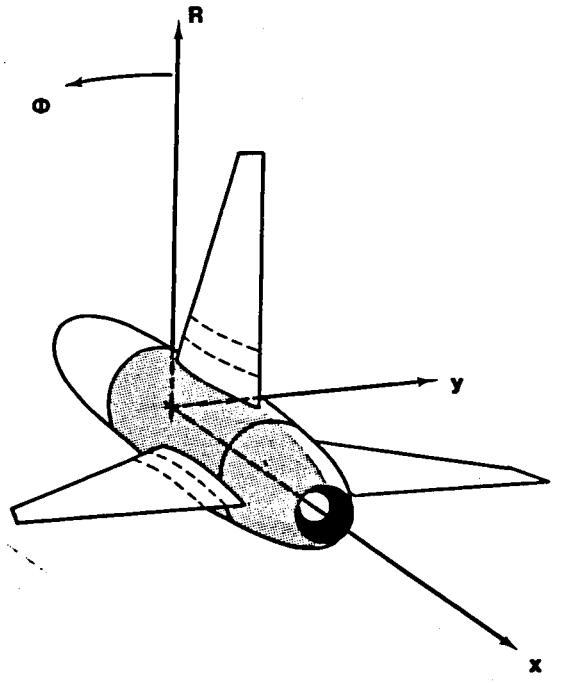

x/l	Φ, deg.											
	0	18	36	45	54	72	81	90	108	135	162	180
.58	●	●		●		●		●	●	●	●	
.60	●	●		●		●		●	●	●	●	
.61	●	●		●		●		●	●	●	●	
.63	●	●		●		●		●	●	●	●	
.64		●		●		●		●	●	●	●	
.65		●		●		●		●	●	●	●	
.67		●		●		●		●	●	●	●	
.68		●		●		●		●	●	●	●	
.70		●		●		●		●	●	●	●	●
.71		●		●		●		●	●	●	●	●
.72		●		●		●		●	●	●	●	●
.74		●		●		●		●	●	●	●	●
.75		●		●		●		●	●	●	●	●
.77		●		●		●		●	●	●	●	●
.78		●		●		●		●	●	●	●	●
.80		●		●		●			●	●	●	●
.81		●		●		●			●	●	●	●
.82		●		●		●			●	●	●	●
.84		●		●		●			●	●	●	●
.85		●		●		●			●	●	●	●
.86		●		●		●			●	●	●	●
.88	●	●		●		●			●	●	●	●
.89	●	●		●		●			●	●	●	●
.92	●	●	●		●	●	●	●	●	●	●	●
.93	●	●	●		●	●	●	●	●	●	●	●
.94	●	●	●		●	●	●	●	●	●	●	●
.95	●	●	●		●	●	●	●	●	●	●	●
.96	●	●	●		●	●	●	●	●	●	●	●
.97	●	●	●		●	●	●	●	●	●	●	●
.99	●	●	●		●	●	●	●	●	●	●	●
1.00	●	●	●		●	●	●	●	●	●	●	●

(b) Pressure orifice locations

Figure 3.- Concluded.

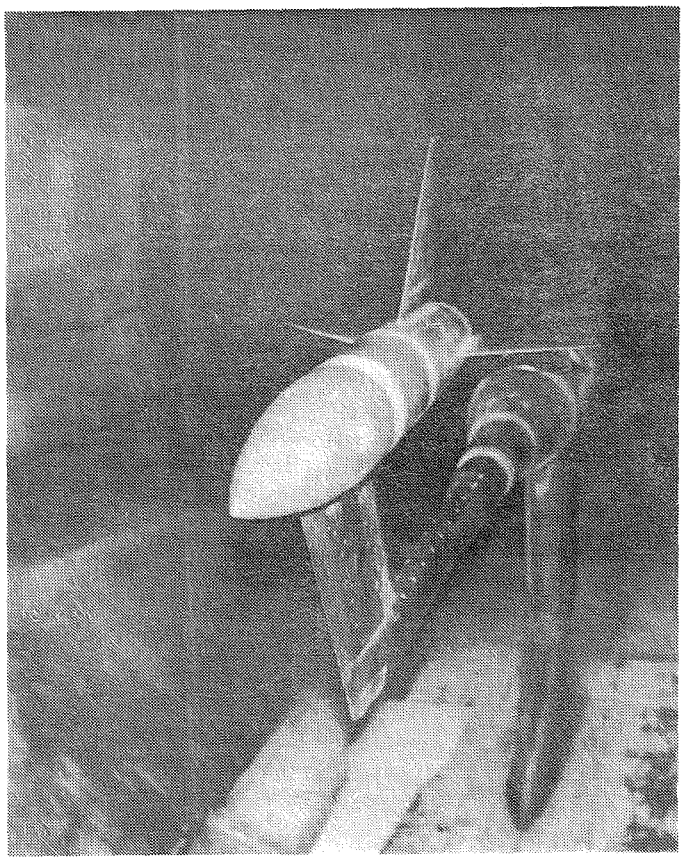

Downstream

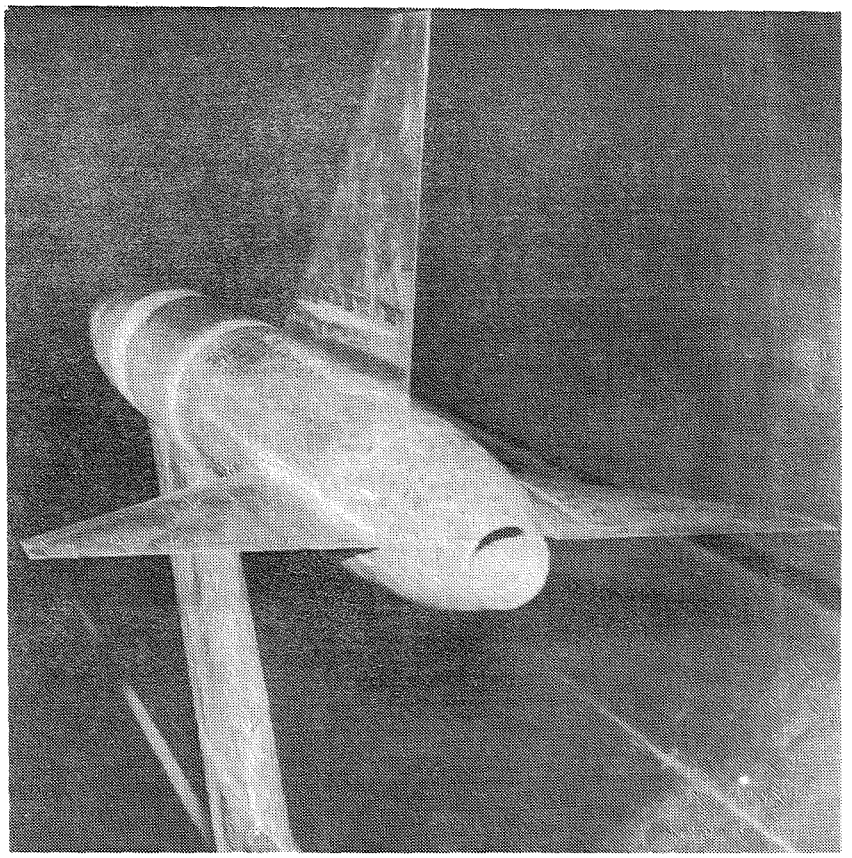

Upstream

Figure 4.- Photographs of the model installed in the 16-Foot transonic tunnel.

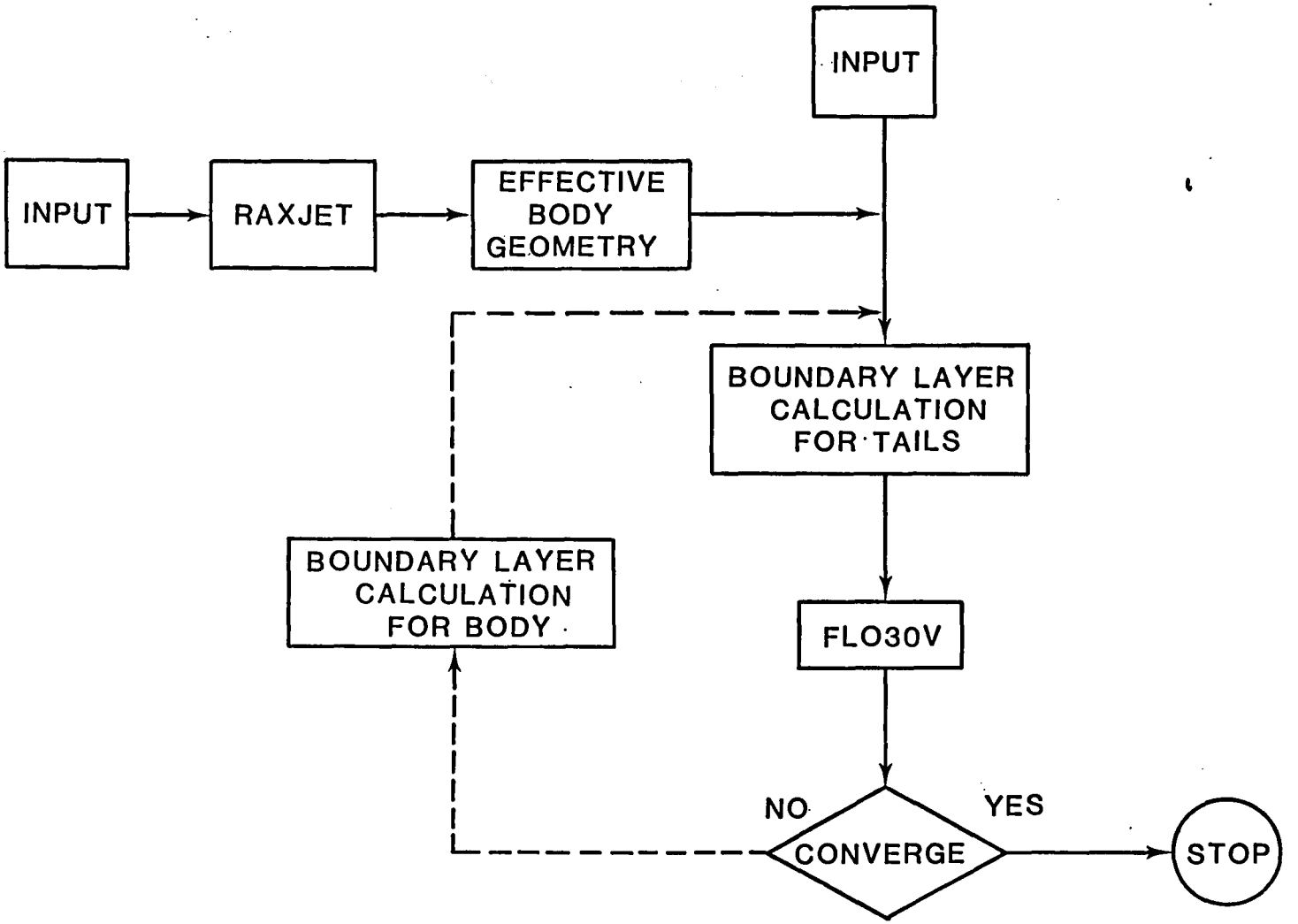

Figure 5. - Viscous-inviscid interaction procedure utilizing RAXJET and FLO30V codes.

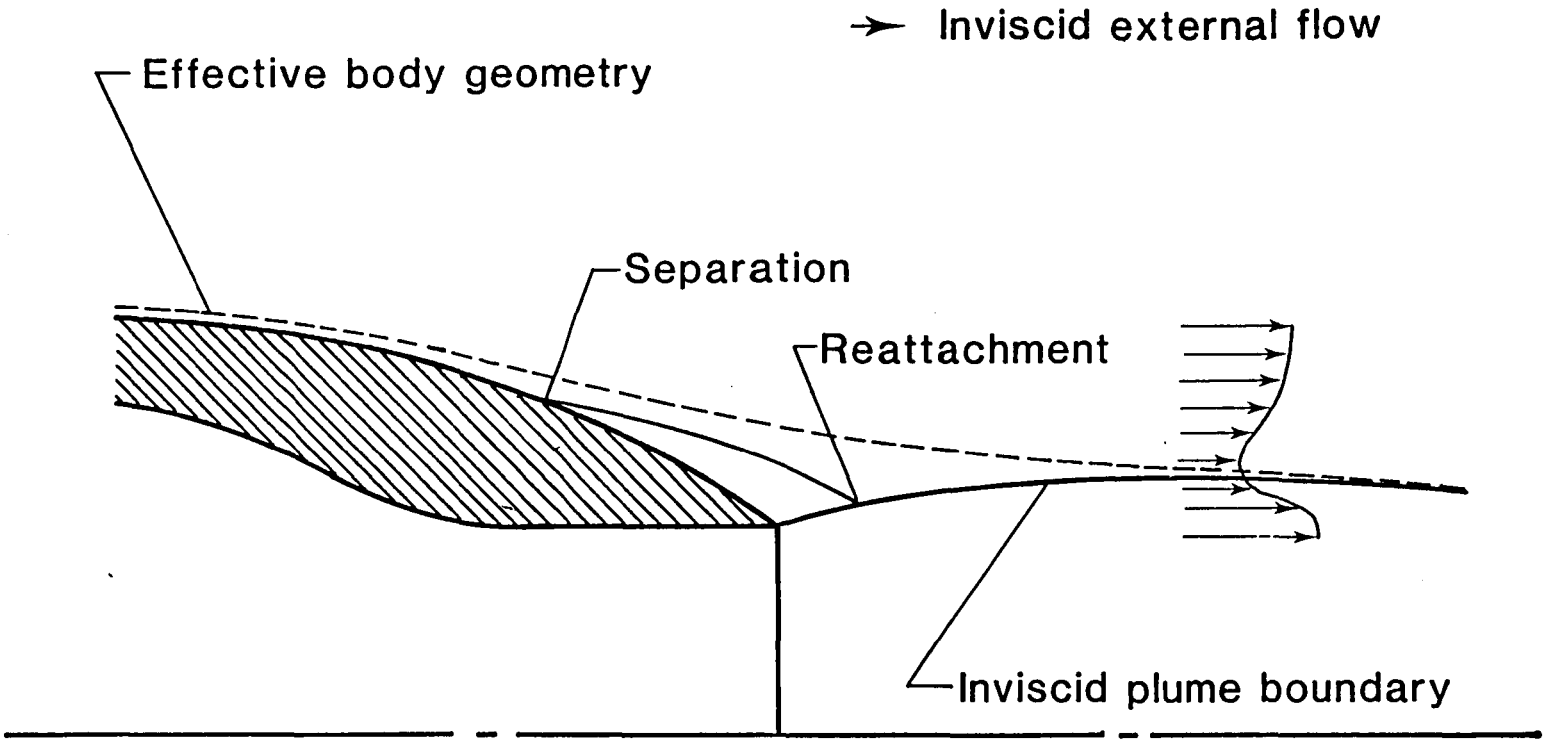

Figure 6. - Flowfield about an axisymmetric nozzle as seen by the RAXJET code.

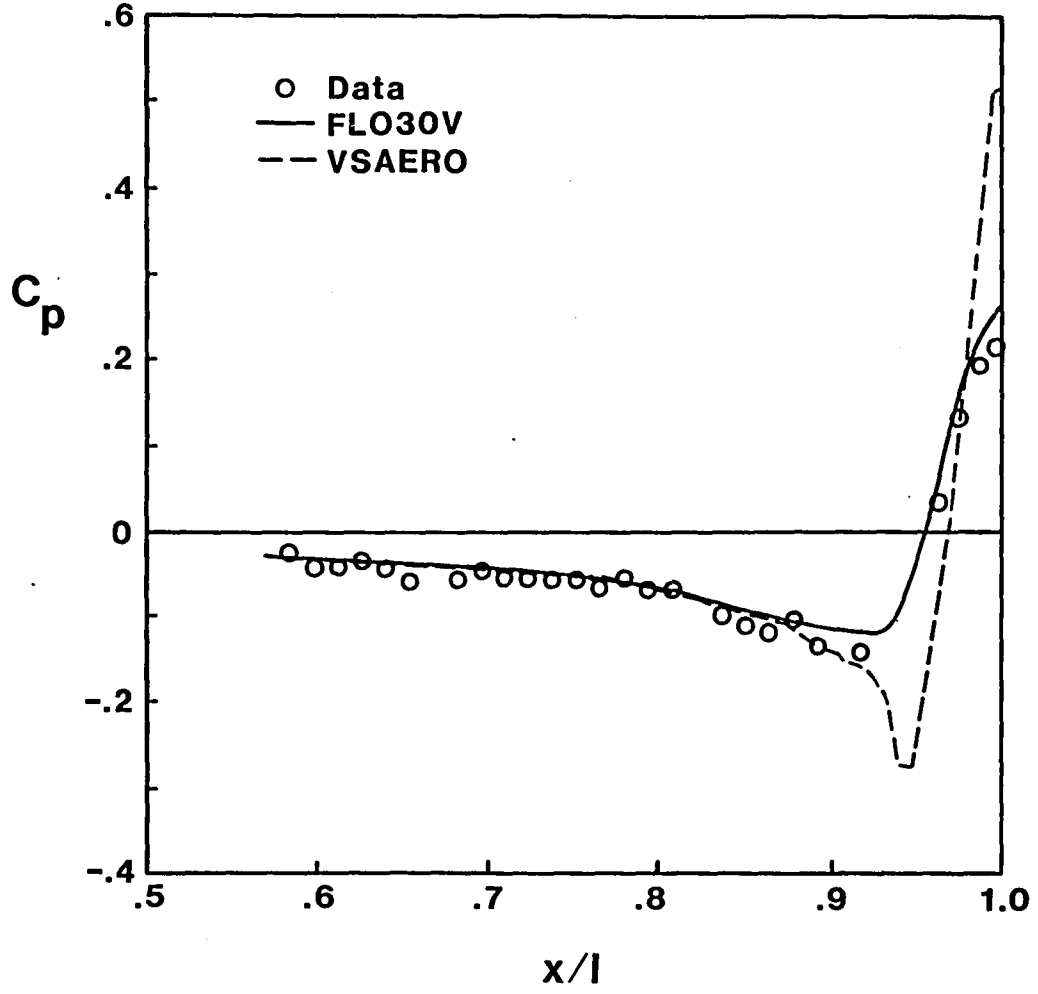

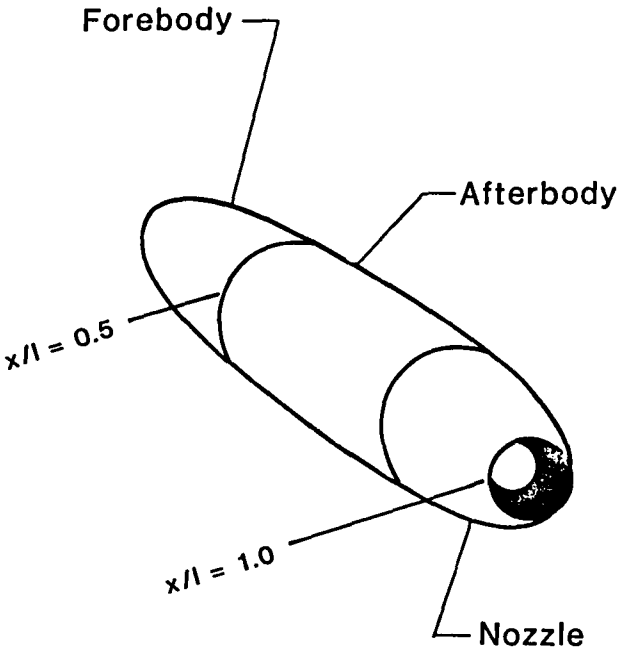

Figure 7. - Comparison of experiemntal and theoretical pressure coefficients on the afterbody and nozzle with the tails removed at M=0.9 and NPR=5.0.

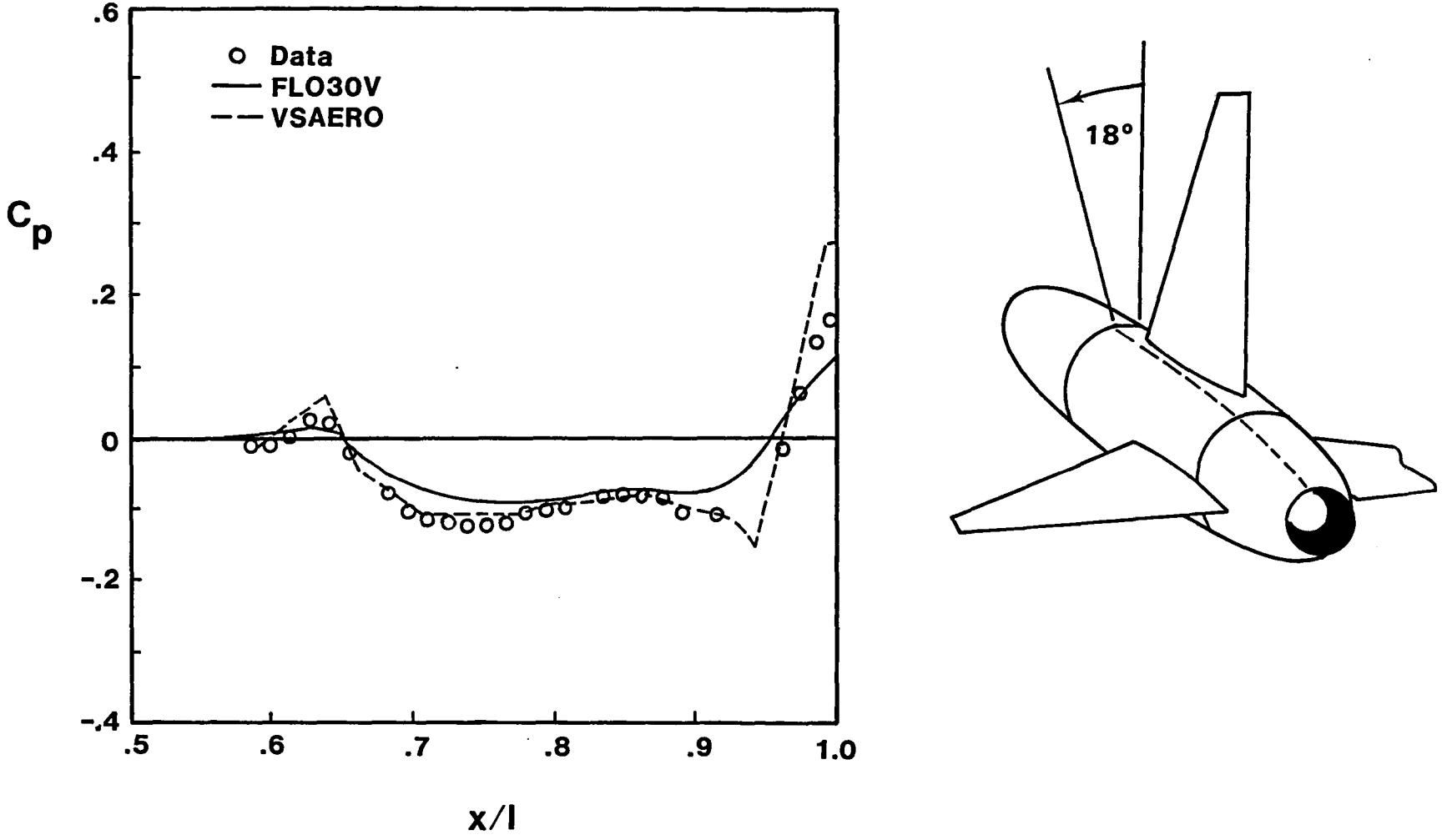

Figure 8. - Comparison of experimental and theoretical pressure coefficients for the staggered empennage arrangement at M=0.6 and NPR=3.0.

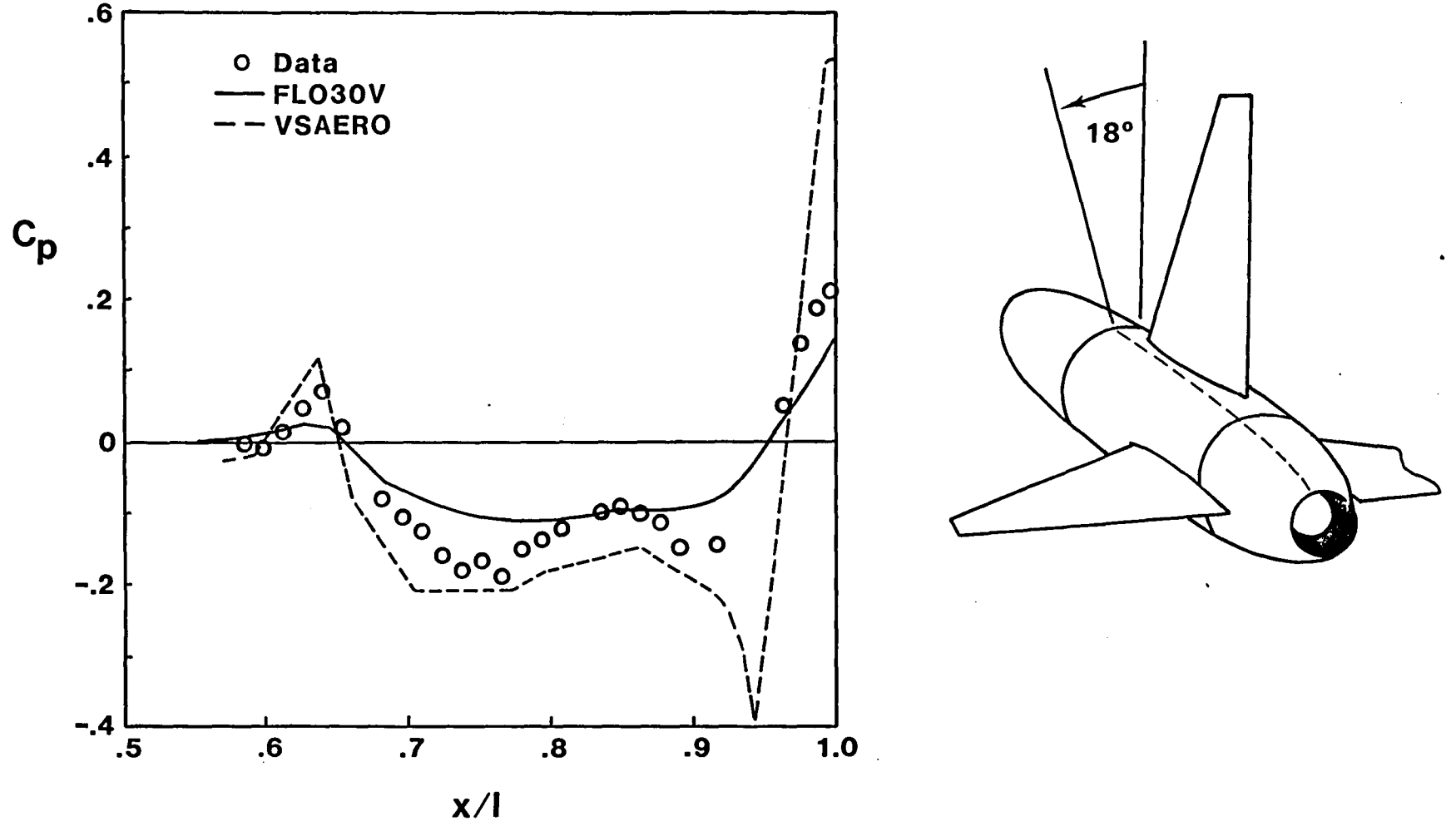

Figure 9. - Comparison of experiemntal and theoretical pressure coefficients for the staggered empennage arrangement at M=0.9 and NPR=5.0.

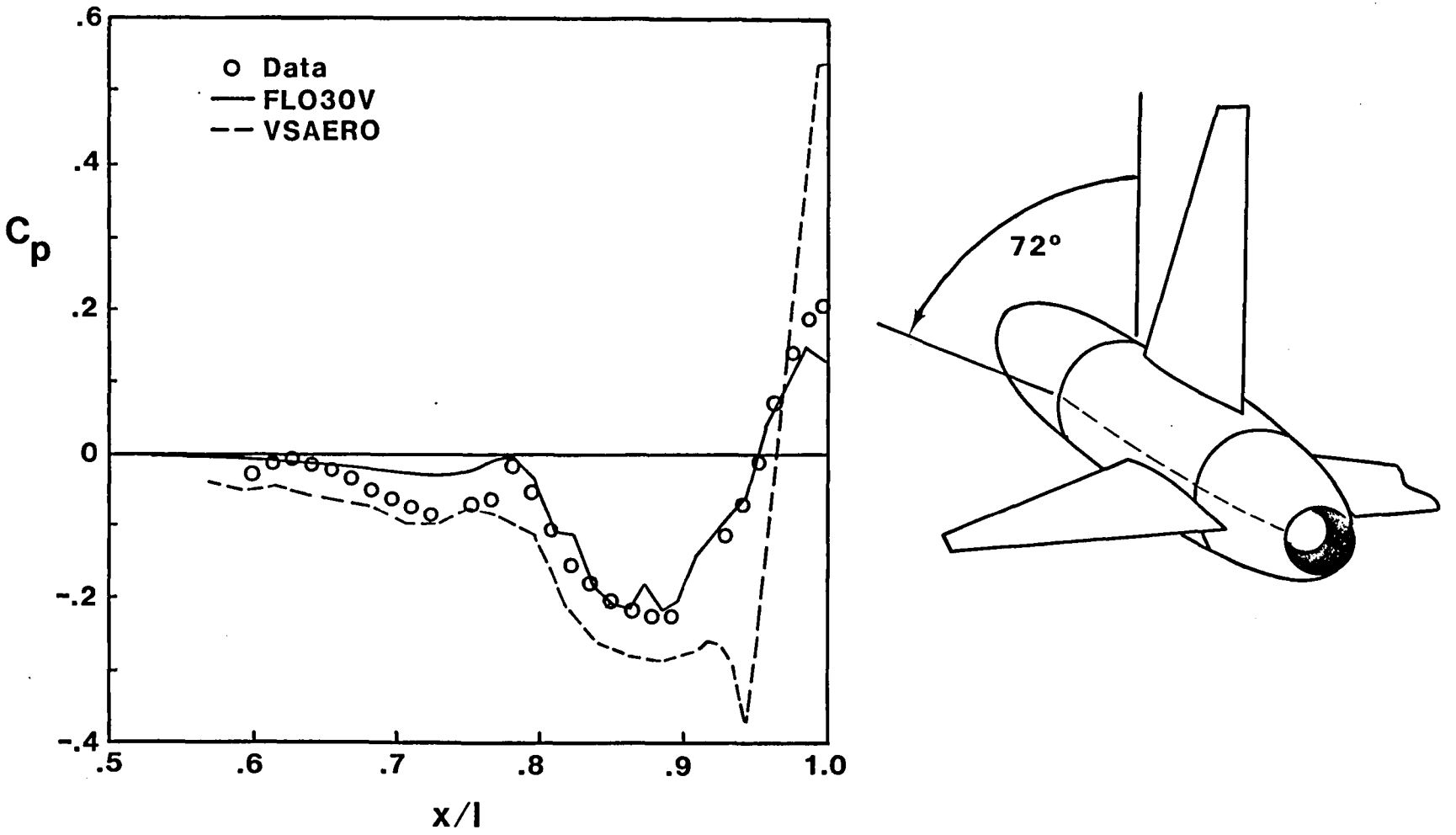

Figure 10. - Comparison of experimental and theoretical pressure coefficients for the staggered empennage arrangement at M=0.9 and NPR=5.0.

Standard Bibliographic Page

1. Report No.	2. Government Accession No.	3. Recipient's Catalog No.
NASA TM-87755		

4. Title and Subtitle	5. Report Date
EXPERIMENTAL AND NUMERICAL RESULTS FOR A GENERIC AXISYMMETRIC SINGLE-ENGINE AFTERBODY WITH TAILS AT TRANSONIC SPEEDS	August 1986
	6. Performing Organization Code: 505-62-91-01
7. Author(s): James R. Burley, II, John R. Carlson, and William P. Henderson	8. Performing Organization Report No.
9. Performing Organization Name and Address: NASA Langley Research Center, Hampton, VA 23665	10. Work Unit No.
	11. Contract or Grant No.
12. Sponsoring Agency Name and Address: National Aeronautics and Space Administration, Washington, DC 20546	13. Type of Report and Period Covered: Technical Memorandum
	14. Sponsoring Agency Code

15. Supplementary Notes

This paper was presented at the AIAA 4th Applied Aerodynamics Conference, June 9-11, 1986, in San Diego, California. AIAA Paper No. 86-1797-CP.

16. Abstract

Static pressure measurements were made on the afterbody, nozzle and tails of a generic single-engine axisymmetric fighter configuration. Data were recorded at Mach numbers of 0.6, 0.9, and 1.2. NPR was varied from 1.0 to 8.0 and angle of attack was varied from -3^{o} to 9^{o}. Experimental data were compared with numerical results from two state-of-the-art computer codes.

17. Key Words (Suggested by Authors(s))	18. Distribution Statement
Pressure Measurements Single-Engine Axisymmetric Transonic Speeds	Unclassified - Unlimited Subject Category 02

19. Security Classif.(of this report)	20. Security Classif.(of this page)	21. No. of Pages	22. Price
Unclassified	Unclassified	19	A02

For sale by the National Technical Information Service, Springfield, Virginia 22161

NASA Langley Form 63 (June 1985)

End of Document